Computer techniques towards the automatic characterization of graphite particles in metallographic images of industrial materials

João P. Papa [a], Rodrigo Y.M. Nakamura [a], Victor Hugo C. de Albuquerque [b], Alexandre X. Falcão [c], João Manuel R.S. Tavares [d],*

[a] Universidade Estadual Paulista, Departamento de Computação, Bauru, Brazil
[b] Programa de Pós-Graduação em Informática Aplicada, Universidade de Fortaleza, Fortaleza, Brazil
[c] Universidade de Campinas, Instituto de Computação, Campinas, Brazil
[d] Faculdade de Engenharia, Universidade do Porto, Porto, Portugal

ABSTRACT

The automatic characterization of particles in metallographic images has been paramount, mainly because of the importance of quantifying such microstructures in order to assess the mechanical properties of materials common used in industry. This automated characterization may avoid problems related with fatigue and possible measurement errors. In this paper, computer techniques are used and assessed towards the accomplishment of this crucial industrial goal in an efficient and robust manner. Hence, the use of the most actively pursued machine learning classification techniques. In particularity, Support Vector Machine, Bayesian and Optimum-Path Forest based classifiers, and also the Otsu's method, which is commonly used in computer imaging to binarize automatically simply images and used here to demonstrated the need for more complex methods, are evaluated in the characterization of graphite particles in metallographic images. The statistical based analysis performed confirmed that these computer techniques are efficient solutions to accomplish the aimed characterization. Additionally, the Optimum-Path Forest based classifier demonstrated an overall superior performance, both in terms of accuracy and speed.

© 2012 Elsevier Ltd. All rights reserved.

1. Introduction

Industrial applications that make use of computer methods of image processing and analysis have grown in the last years, once that are efficient, robust, accurate, non-subjective and can be easily integrated into solutions of inspection and characterization based on images. Metwalli (1986), for instance, has considered the effect of surface quality on the spectral density of laser-speckle images aiming to study the elastic and plastic deformations. Yoon, Lee, Chung, and Kim (2008) presented an effective fault inspection system to identify film defects using image segmentation techniques. Li (2009) applied a Support Vector Machine (SVM) based classifier (Cortes & Vapnik, 1995) to the automatic inspection of local defects embedded in homogeneous copper clad laminate surfaces. Torres-Treviño, Reyes-Valdes, López, and Praga-Alejo (2011) optimized the welding process by the estimation of the Pareto optimal set. Liao (2008) investigated the imbalanced data problem in the classification of different types of weld flaws. Zapata, Vilar, and Ruiz (2011) described an automatic system to detect, recognize, and classify welding defects in radiographic images using an artificial neuronal network (ANN) and an adaptive-network-based fuzzy inference system. Valavanis and Kosmopoulos (2010) used SVM, ANN and *k*-nearest neighbor (*k*-NN) classifiers for the detection and classification of defects in weld radiographs.

Computer methods of image processing and analysis have been applied in order to characterize microstructures in metallic materials; examples include the segmentation and quantification of white cast iron microstructures using mathematical morphology combined with an ANN (Albuquerque, Tavares, & Cortez, 2010), quantification of the porosity in microscopy-based images of synthetic materials using an ANN (Albuquerque, Filho, Cavalcante, & Tavares, 2010; Albuquerque, Papa, Falcão, Filho, & Tavares, 2010), Brinell and Vickers values determination from hardness indentation images based on an automatic image segmentation method (Filho, Cavalcante, Albuquerque, & Tavares, 2010) and graphite nodules shape characterization using a ANN (Scozzafava, Tomesani, & Zucchelli, 2004).

In cast irons, the fracture toughness and ductility strongly depend on the quantity, size and shape of the graphite particles, in which spheroidal graphite improve these properties, whereas more elongated particles or ones with irregular borders are detrimental due to stress concentration points (West, 2008).

* Corresponding author.
   E-mail addresses: papa@fc.unesp.br (J.P. Papa), rodrigo.mizobe@fc.unesp.br (R.Y.M. Nakamura), victor.albuquerque@fe.up.pt (V.H.C. de Albuquerque), afalcao@ic.unicamp.br (A.X. Falcão), tavares@fe.up.pt (João Manuel R.S. Tavares).

Hence, nodular cast iron has superior properties than lamellar irons, especially in terms of tensile strength and strain. Furthermore, cast irons offer a reasonable resistance against corrosion. In general, the mechanical properties are inferior than those of cast or wrought steels, especially when loaded in tension. In compression, high loads can be supported.

The main advantages of cast irons are their low price and ability to originate products of complex shapes, frequently in a single production step. Therefore, cast irons have been often used in numerous industrial applications, such in base structures of manufacturing machines, rollers, valves, pump bodies and mechanical gears. The main families of cast irons are classified according to the shapes of its graphite particles, mainly: nodular cast iron, malleable cast iron, gray cast iron and white cast iron (Callister, 2006). Their properties, as of all materials, are influenced by their microstructure and therefore, its correct characterization is extremely important. Thus, the metallographic based evaluation of materials is commonly used to determine the quantity, appearance, size and distribution of their phases and constituents (Gomes & Paciornik, 2005). In order to carry on the referred evaluation, human visual inspection of the microstructures are usually done based on metallographic samples. However, manual microstructural characterization is an exhausting task because the specialists spend much time exposed to high luminosities in the microscope device, which can produce fatigue and, consequently, increase the probability of measurement errors (Albuquerque, Cortez, de Alexandria, & Tavares, 2008; Albuquerque, de Alexandria, Cortez, & Tavares, 2009). Another point that should be stressed is the subjectivity inherent to the manual characterization, which may lead to different evaluations for the same metallographic sample.

In order to overcome the aforementioned drawbacks, we aimed the automatic graphite particles characterization of cast irons from high resolution metallographic images, using computer methods. The main contribution of this paper is to present a comparison among the state-of-the-art computer classifiers to accomplish this task, such as Support Vector Machine, Optimum-Path Forest (OPF) (Papa, Falcão, & Suzuki, 2009) and Bayesian based classifiers (Duda, Hart, & Stork, 2000). Additionally, as far as we know, we are the first to apply OPF, SVM and Bayesian based classifiers in the context of graphite particles automatic image based characterization. We also compared the results obtained by the Otsu's method (Otsu, 1979). The Otsu's method was used here to demonstrate that the classifiers, although their superior computer complexity, are more robust and efficient.

The remainder of this paper is organized as follows. Section 2 revisits the computer classifiers used. Section 3 addresses the experimental results and Section 4 states the conclusions.

2. Computer classifiers

This section addresses a review about the computer classifiers under comparison: Support Vector Machine, Optimum-Path Forest and Bayesian based classifiers.

2.1. Support Vector Machine based classifier

Let $\mathcal{X}$ be a training set where each sample $\mathcal{X}_i \in \Re^n$ may be associated to a label $y_i = \{+1, -1\}$. One of the fundamental problems of the computer learning theory is stated as: given two classes of known objects, assign one of them to a new unknown object. Thus, the objective in a two-class pattern recognition is to infer a function (Scholköpf & Smola, 2002):

$$f : \mathcal{X} \to \{\pm 1\}, \tag{1}$$

regarding the input–output of the training data.

Based on the principle of *structural risk minimization* (Vapnik, 1999), the SVM optimization process is aimed at establishing a separating function while accomplishing with the trade-off that exists between generalization and overfitting. Vapnik (1999) considered the class of hyperplanes in some dot product space $\mathcal{H}$:

$$\langle \mathbf{w}, \mathbf{x} \rangle + b = 0, \tag{2}$$

where $\mathbf{w}, \mathbf{x} \in \mathcal{H}, b \in \mathbb{R}$, corresponding to the decision function:

$$f(x) = \text{sgn}(\langle \mathbf{w}, \mathbf{x} \rangle + b), \tag{3}$$

in which *sgn* stands for the signal function. Based on the following two arguments, the author proposed the *Generalized Portrait* learning algorithm for problems which are separable by hyperplanes:

1. Among all hyperplanes separating the data, there exists a unique *optimal hyperplane* defined by the maximum margin of separation between any training point and the hyperplane;
2. The overfitting of the separating hyperplanes decreases with margin increasing.

Thus, to obtain the optimal hyperplane, it is necessary to solve:

$$\underset{\mathbf{w} \in \mathcal{H}, b \in \mathbb{R}}{minimize} \quad \tau(\mathbf{w}) = \frac{1}{2} \|\mathbf{w}\|^2, \tag{4}$$

subject to:

$$y_i(\langle \mathbf{w}, \mathbf{x}_i \rangle + b) \geqslant 1 \quad \text{for all} \quad i = 1, \ldots, m, \tag{5}$$

with constraints given by Eq. (5) ensuring that $f(x_i)$ will be +1 for $y_i = +1$ and -1 for $y_i = -1$, and also fixing the scale of $\mathbf{w}$. A wide exposition of these arguments is provided by Scholköpf and Smola (2002).

The function τ in Eq. (4) is called the *objective function*, while the constraints given by Eq. (5) are the *inequality constraints*. Together, they form a so-called *constrained optimization problem*. The separating function is then a weighted combination of elements of the training set. These elements are called *Support Vectors* and characterize the boundary between the two classes.

The replacement referred to as the *kernel trick* (Scholköpf & Smola, 2002) is used to extend the concept of hyperplane classifiers to nonlinear Support Vector Machine based classifiers. However, even with the advantage of "kernelizing" the problem, the separating hyperplane may still not exist.

In order to allow that some cases may violate Eq. (5), the slack variables $\xi \geqslant 0$ were introduced (Scholköpf & Smola, 2002), which leads to the new constraints:

$$y_i(\langle \mathbf{w}, \mathbf{x}_i \rangle + b) \geqslant 1 - \xi_i \quad \text{for all} \quad i = 1, \ldots, m. \tag{6}$$

A computer classifier that generalizes well is then found by controlling both the margin (through $\|\mathbf{w}\|$) and the sum of the slacks variables $\sum_i \xi_i$. As such, a possible accomplishment of such a *soft margin* classifier is obtained by minimizing the objective function:

$$\tau(\mathbf{w}, \xi) = \frac{1}{2} \|\mathbf{w}\|^2 + C \sum_{i=1}^{m} \xi_i, \tag{7}$$

subject to the constraints given by Eq. (6) and $\xi \geqslant 0$, where the constant $C > 0$ determines the balance between overfitting and generalization. Due to the tunning variable C, these kinds of SVM based classifiers are normally referred to as C-Support Vector Classifiers (C-SVC) (Cortes & Vapnik, 1995).

However, the above formulation can be applied only for linearly separable feature spaces. Boser, Guyon, and Vapnik (1992) have proposed an extension for non-linearly separable situations by applying the kernel trick to maximum-margin hyperplanes. The idea is to replace the dot product in Eq. (6) by a nonlinear kernel function:

$$y_i(K(w,x_i) + b) \geqslant 1 - \xi_i \quad \text{for all} \quad i = 1, \ldots, m. \tag{8}$$

It is important to highlight that the choice of kernel function strongly depends on the problem. Some common kernels that have been used are:

- $K(x_i, x_j) = (x_i \cdot x_j + 1)^p$ (polynomial kernel);
- $K(x_i, x_j) = \exp -\frac{\|x_i - x_j\|^2}{2\sigma^2}$ (Gaussian radial basis function kernel);
- $K(x_i, x_j) = \tanh(a x_i \cdot x_j + b, a > 0 \text{ and } b < 0)$ (hyperbolic tangent).

in which x_i and x_j stand for the samples, p is the polynomial degree and σ is the Gaussian variance.

2.2. Optimum-Path Forest based classifier

The OPF based classifier works by modeling the problem of computer classification as a graph partition in a given feature space. The nodes are represented by the feature vectors and the edges connect all pairs of them, defining a full connectedness graph. This kind of representation is straightforward, given that the graph does not need to be explicitly represented, allowing the saving of computer memory. The partition of the graph is carried out by a competition process between some key samples (prototypes), which offer optimum paths to the remaining nodes of the graph. Each prototype sample defines its optimum-path tree (OPT), and the collection of all OPTs defines the Optimum-Path Forest, which gives the name to the classifier (Papa et al., 2009).

The OPF can be seen as a generalization of the well known Dijkstra's algorithm to compute optimum paths from a source node to the remaining ones (Dijkstra, 1959). The main difference relies on the fact that OPF uses a set of source nodes (prototypes) with any path-cost function. In case of Dijkstra's algorithm, a function that summed the arc-weights along a path was applied. For OPF, we used a function that gives the maximum arc-weight along a path, as is explained below.

Let $Z = Z_1 \cup Z_2$ be a dataset labeled with a function λ, in which Z_1 and Z_2 are, respectively, a training and test sets, and let $S \subseteq Z_1$ be a set of prototype samples. Essentially, the OPF based classifier creates a discrete optimal partition of the feature space such that any sample $s \in Z_2$ can be classified according to this partition. This partition is an optimum path forest (OPF) computed in $\Re^n$ by the image foresting transform (IFT) algorithm (Falcão, Stolfi, & Lotufo, 2004).

The OPF algorithm may be used with any smooth path-cost function which can group samples with similar properties (Falcão et al., 2004). Particularly, we use the path-cost function f_{max} that is computed as:

$$f_{max}(\langle s \rangle) = \begin{cases} 0 & \text{if } s \in S, \\ +\infty & \text{otherwise} \end{cases}$$
$$f_{max}(\pi \cdot \langle s,t \rangle) = \max\{f_{max}(\pi), d(s,t)\}, \tag{9}$$

in which $d(s,t)$ means the distance between samples s and t, and a path π is defined as a sequence of adjacent samples. As such, we have that $f_{max}(\pi)$ computes the maximum distance between adjacent samples in π, when π is not a trivial path. The choice for f_{max} arises from the fact of avoiding the "chain code problem", because does not matter the size of the path connecting samples, since the arc-weight between them be small.

The OPF algorithm assigns one optimum path $P^*(s)$ from S to every sample $s \in Z_1$, building an optimum path forest P (a function with no cycles which assigns to each $s \in Z_1 \backslash S$ its predecessor $P(s)$ in $P^*(s)$ or a marker nil when $s \in S$).

The OPF based classifier has two distinct phases: (i) training and (ii) classification. The former phase consists, essentially, into finding the prototypes and computing the Optimum-Path Forest, which is the union of all OPTs rooted at each prototype. After that, a sample is selected from the test sample, connect it to all samples of the Optimum-Path Forest generated in the training phase and the node associated the optimum path to it is found. Notice that this test sample is not permanently added to the training set, i.e., only used once. The next sections describe in more detail the two classifier phases.

2.2.1. Training

We say that S^* is an optimum set of prototypes when OPF Algorithm minimizes the classification errors for every $s \in Z_1$. S^* can be found by exploiting the theoretical relation between minimum-spanning tree (MST) and optimum-path tree for f_{max} (Allène, Audibert, Couprie, Cousty, & Keriven, 2007). The training essentially consists in finding S^* and an OPF classifier rooted at S^*.

By computing an MST in the complete graph (Z_1, A), we obtain a connected acyclic graph whose nodes are all samples of Z_1 and the arcs are undirected and weighted by the distances d between adjacent samples. The spanning tree is optimum as that the sum of its arc weights is minimum as compared to any other spanning tree in the complete graph. In the MST, every pair of samples is connected by a single path which is optimum according to f_{max}. That is, the minimum-spanning tree contains one optimum-path tree for any selected root node. Thus, the optimum prototypes are the closest elements of the MST with different labels in Z_1; elements that fall in the frontier of the classes.

After finding the prototypes, they will compete among themselves in order to conquer the remaining training nodes offering to them optimum-path costs, which are computed using Eq. (9). Suppose we have path τ between $s \in S$ and $t \in Z_1$: Eq. (9) refers that the cost offered to t by s is the maximum arc-weight along τ. Therefore, the prototype that will conquer t will be the one that presents the minimum path-cost.

2.2.2. Classification

For any sample $t \in Z_2$, we consider all arcs connecting t with samples $s \in Z_1$, as though t were part of the training graph. Considering all possible paths from S^* to t, we find the optimum path $P^*(t)$ from S^* and label t with the class $\lambda(R(t))$ of its most strongly connected prototype $R(t) \in S^*$. This path can be identified incrementally by evaluating the optimum cost $C(t)$ as:

$$C(t) = \min\{\max\{C(s), d(s,t)\}\}, \quad \forall s \in Z_1. \tag{10}$$

Let the node $s^* \in Z_1$ be the one that satisfies Eq. (10); i.e., the predecessor $P(t)$ in the optimum path $P^*(t)$. Given that $L(s^*) = \lambda(R(t))$, the classification simply assigns $L(s^*)$ as the class of t. An error occurs when $L(s^*) \neq \lambda(t)$.

2.3. Bayesian based classifier

Let $p(\omega_i|x)$ be the probability of a given pattern $x \in \Re^n$ to belong to class ω_i, $i = 1, 2, \ldots, c$, which can be defined by the Bayes Theorem (Jaynes, 2003):

$$p(\omega_i|x) = \frac{p(x|\omega_i)P(\omega_i)}{p(x)}, \tag{11}$$

where $p(x|\omega_i)$ is the probability density function of the elements that compose the class ω_i, and $P(\omega_i)$ corresponds to the probability of the class ω_i itself.

A Bayesian based classifier decides whether a pattern x belongs to the class ω_i when:

$$p(\omega_i|x) > p(\omega_j|x), \quad i,j = 1, 2, \ldots, c, \ i \neq j, \tag{12}$$

which can be rewritten as follows by using Eq. (11):

$$p(x|\omega_i)P(\omega_i) > p(x|\omega_j)P(\omega_j), \quad i,j = 1, 2, \ldots, x, \ i \neq j. \tag{13}$$

As one can see, the Bayes classifier's decision function $d_i(x) = p(x|\omega_i)P(\omega_i)$ of a given class ω_i strongly depends on the previous knowledge of $p(x|\omega_i)$ and $P(\omega_i)$, $\forall i = 1,2,\ldots,c$. The probability values of $P(\omega_i)$ are straightforward obtained by calculating the histogram of the classes, for instance. However, the main problem associated to the Bayesian based classifiers is to find the probability density function $p(x|\omega_i)$, given that the only information we have is a set of classes and its corresponding labels. A common practice is to assume that the probability density functions are Gaussian ones, and thus one can estimate their parameters using the dataset samples (Duda et al., 2000). In the n-dimensional case, a Gaussian density of the patterns from class ω_i can be calculated using:

$$p(x|\omega_i) = \frac{1}{(2\pi)^{n/2}|C_i|^{1/2}} exp\left[-\frac{1}{2}(x - \mu_i)^T C_i^{-1}(x - \mu_i)\right], \tag{14}$$

in which μ_i and C_i correspond to the mean and the covariance matrix of class ω_i. These parameters can be obtained by considering each element x that belongs to class ω_i using:

$$\mu_i = \frac{1}{N_i}\sum_{x \in \omega_i} x \tag{15}$$

and

$$C_i = \frac{1}{N_i}\sum_{x \in \omega_i}(xx^T - \mu_i\mu_i^T), \tag{16}$$

in which N_i means the number of samples from class ω_i.

3. Experiments

In this section, we describe the dataset addressed, the computer classifiers used and explain the experiments conducted in order to automatic characterize three types of ferrous alloy samples: nodular, gray and malleable cast irons.

3.1. Datasets

For the application of the computer methods used and under comparison here, firstly, it was necessary the metallographic preparation of the cast iron samples under study. Then, the samples were microscopically analyzed, accomplishing with suitable brightness and contrast adjustments, and the correspondent images were acquired. We used a collection of three labeled images of each cast iron for quantitative evaluation (Fig. 1), each one manually characterized by an expert.

As we are regarding the characterization of each pixel in the input images, each pixel has been described by a texture kernel around its neighborhood and also by its gray value. Taking this into account, in order to extract the texture information, we applied the Gabor filter (Feichtinger & Strohmer, 1997), which can be mathematically formulated as:

$$G(x,y,\theta,\gamma,\sigma,\lambda,\psi) = e^{-\frac{x'^2+\gamma^2 y'^2}{2\sigma^2}} e^{i\left(2\pi\frac{x'}{\lambda}+\psi\right)}, \tag{17}$$

where $x' = x\cos(\theta) + y\sin(\theta)$ and $y' = x\sin(\theta) + y\cos(\theta)$, and λ means the sinusoidal factor, θ represents the orientation angle, ψ is the phase offset, σ is the Gaussian standard deviation and γ is the aspect spatial ratio.

The main idea of the Gabor filter is to perform a convolution between the original image I and $G_{\theta,\gamma,\sigma,\lambda,\psi}$ in order to obtain a Gabor-filtered representation:

$$\widehat{I}_{\theta,\gamma,\sigma,\lambda,\psi} = I * G_{\theta,\gamma,\sigma,\lambda,\psi}, \tag{18}$$

in which $\widehat{I}_{\theta,\gamma,\sigma,\lambda,\psi}$ denotes the filtered image. Thus, one can obtain a filter bank of Gabor filtered images by varying its parameters. In this work, we used a convolution filter of size 3×3 with the following Gabor parameters:

- Six different orientations: $\theta = 0°$, $45°$, $90°$, $135°$, $225°$ and $315°$;
- Three spatial resolutions: $\lambda = 2.5$, 3 and 3.5. Notice that, for each one of λ values, we applied different values for σ: 1.96, 1.40 and 1.68;
- $\psi = 0$;
- $\gamma = 1$.

These values were empirically chosen based on our previous experience Pisani et al. (2011), Pisani, Riedel, Gomes, Nakamura, and Papa (2011), Papa et al. (2011).
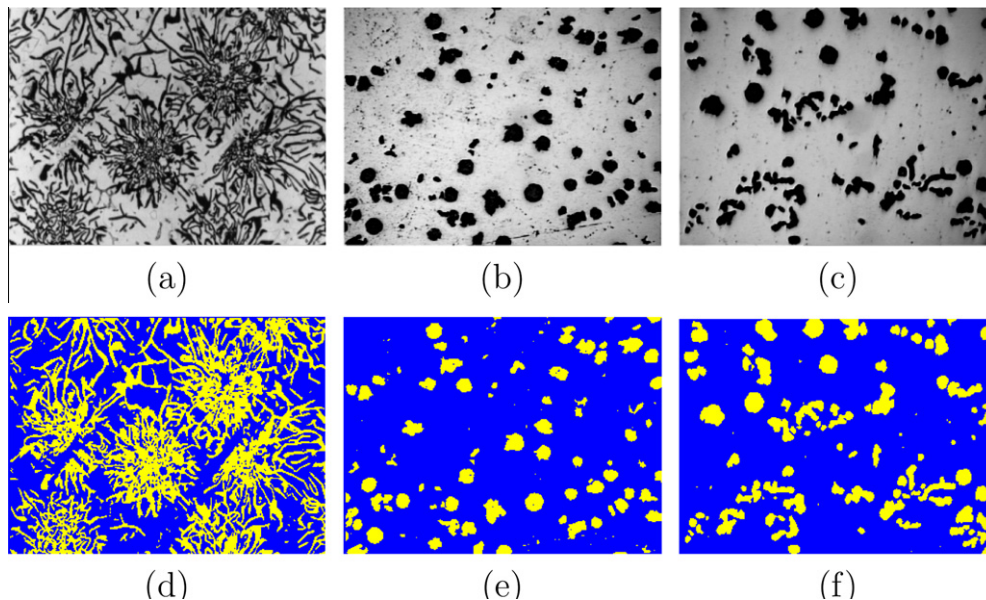
Fig. 1. Microstructure images of cast irons: (a) gray, (b) nodular and (c) malleable and their respective labeled (manually characterized), images in (d), (e) and (f). All images shown in this paper have 320×240 pixels and are according a magnification factor of $100\times$.

Once we get the Gabor-filtered images (notice that we have used $6 \times 3 = 18$ images), we then compute the texture features at pixel p as the set of corresponding gray values among these images. Thus, each pixel is described by 19 features, being 18 of them related with texture and the remaining one is the original gray value. After the classification process, we applied a 3×3 mode filter in order to post-processing the resultant image.

In regard to the computer classifiers, we have applied and evaluated the SVM with Radial Basis Function (SVM-RBF), OPF and Bayesian (Bayes) based classifiers. For the OPF based classifier we employed LibOPF Papa, Suzuki, and Falcão (2009), which is a free tool to the design computer classifiers based on Optimum-Path Forest, and for the Bayes based classifier we used our own computer implementation. Finally, with respect to the SVM-RBF based classifier, we have applied SVMTorch Collobert and Bengio (2001).

In addition, we compare the results obtained by the aforementioned machine learning techniques against the Otsu's method Otsu (1979), which has been commonly used in computer image processing to segment images. This segmentation technique aims to automatic estimate a threshold based on the image's histogram shape. The algorithm assumes that the image to be thresholded contains two classes of pixels or a bi-modal histogram (foreground and background classes), and then it calculates the optimum threshold that separates those two classes so that their intraclass variance is minimal Sezgin and Sankur (2004).

3.2. Experimental results

In this section, we present the results obtained in the automatic characterization of the graphite particles in metallographic images of cast irons. The accuracy of the computer methods under comparison were assessed by the Universal Image Quality Index (UIQI) Wang and Bovik (2002), which considers the brightness variance of the image pixels over a neighborhood, as follows:

$$UIQI = \frac{4\sigma_{xy}\overline{x}\overline{y}}{\left(\sigma_x^2 + \sigma_y^2\right)(\overline{x}^2 + \overline{y}^2)}, \qquad (19)$$

in which $\overline{x}$, $\overline{y}$, σ_x^2 and σ_y^2 are the average and variance of each image under comparison, respectively, and the σ_{xy} is the correlation coefficient between x and y. The dynamic range of UIQI is $[-1,1]$, and the best value is achieved when $y = x$; i.e., the two images under comparison are similar.

Table 1 indicates the mean UIQI values obtained as well as their standard deviations, and the required times by the computer methods under comparison in the characterization of malleable, gray and nodular cast irons. For the malleable and nodular cast irons, we used 10% of the correspondent image shown in Fig. 1b-c for training and the remaining 90% for testing the computer classifiers. In regard to the gray cast iron (Fig. 1a), we employed 50% for training and 50% for testing, since we have observed that this cast iron revealed to be the most difficult to characterize due to the high complexity of the related image. Notice for all cast irons we have employed a cross-validation over 10 runnings. All experiments were conducted using a personal computer with a Pentium Intel Core i7®, 4 GB of RAM and GNU/Linux Gentoo as the operational system. Fig. 2 displays the results obtained by all computer methods under comparison.

In Fig. 2, one can clearly see that the quantitative results agree well with the visual analysis. Also, the Otsu's optimal threshold obtained a good result for the gray cast iron; however, the computer classifiers outperform it for the nodular cast iron. In regard to malleable cast iron, the Otsu's method was slightly better than the computer classifiers.

In order to perform a statistical analysis, we compared all possible pairwise combination of computer methods using the

Table 1
Mean UIQI and execution times in seconds after cross-validation for OPF, SVM-RBF and Bayes based classifiers and for Otsu's method in the cast iron characterization. (The most accurate results are in bolded.)

| Classifier	Cast iron	UIQI	Training [s]	Testing [s]
OPF	Gray	−0.0050 ± 0.0033	128.13	230.14
Bayes	Gray	−0.0034 ± 0.0036	35.25	286.32
SVM-RBF	Gray	0.0010 ± 0.0025	3892.33	155.30
Otsu	Gray	**0.16964**	0.038	
OPF	Nodular	**0.8516 ± 0.0061**	**4.21**	**18.97**
Bayes	Nodular	**0.8591 ± 0.0049**	**0.52**	**45.46**
SVM-RBF	Nodular	0.8281 ± 0.0028	2.47	11.21
Otsu	Nodular	0.64642	0.018	
OPF	Malleable	0.5023 ± 0.0150	4.28	35.80
Bayes	Malleable	0.5417 ± 0.0128	0.61	35.51
SVM-RBF	Malleable	0.5253 ± 0.0113	2.82	10.47
Otsu	Malleable	**0.6877**	0.048	

McNemar test (Kuncheva, 2004). As such, the value of χ^2 was computed as:

$$\chi^2 = \frac{((N_{01} - N_{10}) - 1)^2}{N_{01} + N_{10}}; \qquad (20)$$

in which N_{01} represents the number of times that a first method misclassifies and a second one gives a correct classification, and N_{10} the number of times that the first method correct classified and the second misclassified. As the null hypothesis, we assumed that both methods had similar performance. Hence, if the value of χ^2 is greater than 10.83 ($p = 0.001$), we can reject the null hypothesis and the computer methods under comparison had distinct performance. Tables 2–4 present the values of χ^2 computed for all pairs of computer methods considering the gray, malleable and nodular cast irons. We have highlighted the pair of classifiers that accepted the null hypothesis (similar classifiers).

One can realize from the values indicated in Table 2 that the null hypothesis is rejected for the gray cast iron for all pairs of computer methods, being the Otsu's method the most accurate, which can be clearly confirmed by observing Fig. 2j.

In regard to the nodular cast iron (Table 3), the most accurate computer methods were the OPF and Bayesian based classifiers, which have accepted the null hypothesis; i.e., both computer classifiers obtained similar effectiveness. However, the OPF based classifier was overall about 2.02 times faster than the Bayesian based classifier. Finally, with respect to the malleable cast iron, the Otsu's method was the most accurate, and the OPF and SVM-RBF based classifiers had similar results according to χ^2 value obtained (Table 4). Although one may argue that the Otsu's threshold has outperformed the machine learning techniques in about 66% of the experiments, there are situations in which the local basis of the Otsu's method can not handle successfully more complex images. In order to illustrate such cases, we have conducted an extra round of experiment with a different gray cast iron image. Fig. 3a and b display, respectively, this new image and its labeled version. In this new round of experiment, we employed the same set of computer classifiers as before against the Otsu's method. Fig. 4 displays the characterized images. Table 5 presents the UIQI results. One can see that OPF and Bays have been the most accurate classifiers, and Table 6 confirms such results, in which the χ^2 value of the pair OPF-Bayes is lower than 10.83. Thus, they accept the null hypothesis, being similar to each other. Analyzing by visual inspection the quality of the characterization results, one can conclude that the by Otsu's method was not effective, since that pearlite or ferrite (that should be classified as background) has been erroneously identified (view at the top and bottom right corner).
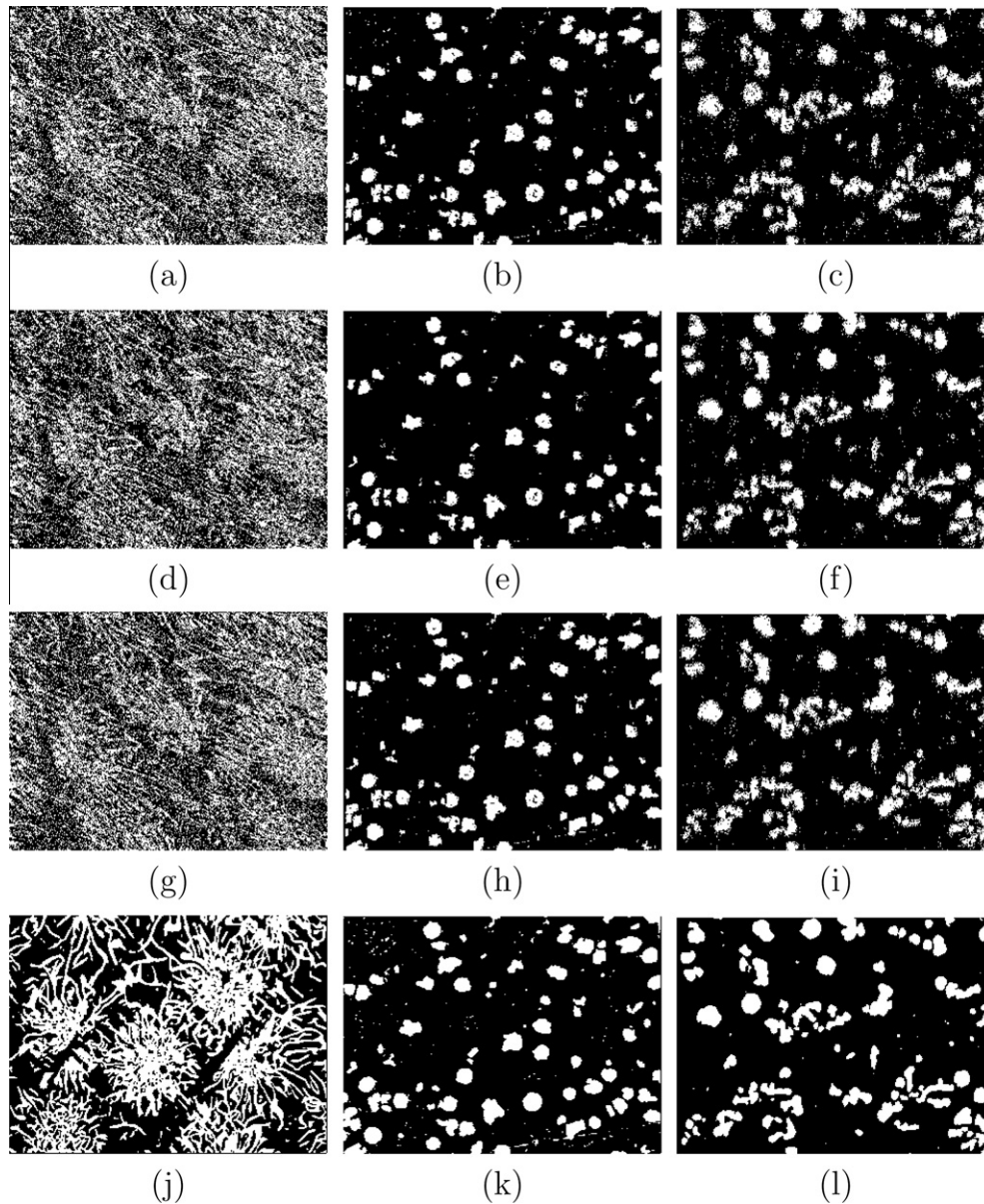
Fig. 2. Image based characterization results: (a)–(c) OPF, (d)–(f) SVM-RBF, (g)–(i) Bayes based classifiers and (j)–(l) Otsu's method. The left images correspond to the gray cast iron, and the middle and right ones correspond to the nodular and malleable cast irons, respectively.

Table 2
Values of χ^2 computed for all pairs of computer methods under comparison for the gray cast iron (Fig. 1a).

χ^2	Bayes	OPF	SVM-RBF	Otsu
Bayes	–	52.612	71.158	10842.0
OPF	52.612	–	28.559	10416.0
SVM-RBF	71.158	28.559	–	9958.6
Otsu	10842.0	10416.0	9958.6	–

Table 3
Values of χ^2 computed for all pairs of computer methods for the nodular cast iron (Fig. 1b). (The bolded values stand for similar classifiers.)

| χ^2	Bayes	OPF	SVM-RBF	Otsu
Bayes	–	**7.5078**	522.57	2631.7
OPF	**7.5078**	–	476.72	2566.8
SVM-RBF	522.57	476.72	–	1295.7
Otsu	2631.7	2566.8	1295.7	–

Table 4
Values of χ^2 computed for all pairs of computer methods under comparison for the malleable cast iron (Fig. 1c). (The bolded values stand for similar classifiers.)

χ^2	Bayes	OPF	SVM-RBF	Otsu
Bayes	–	194.68	19.152	37.865
OPF	194.68	–	**1.7673**	110.92
SVM-RBF	19.152	**1.7673**	–	88.056
Otsu	37.865	110.92	88.056	–

4. Conclusions

In this paper, we addressed the problem of automatic characterization of cast iron in metallographic images; in particular, three types of cast iron were considered: nodular, gray and malleable. Given that the analysis of the microstructures present in materials may lead to several evaluations, their identification for further
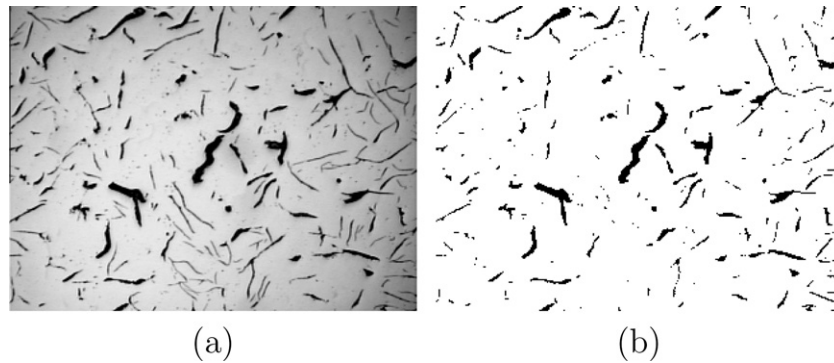
Fig. 3. Gray cast iron images employed in the second round of experiments: (a) original and (b) labeled version by an specialist in microstructural characterization.
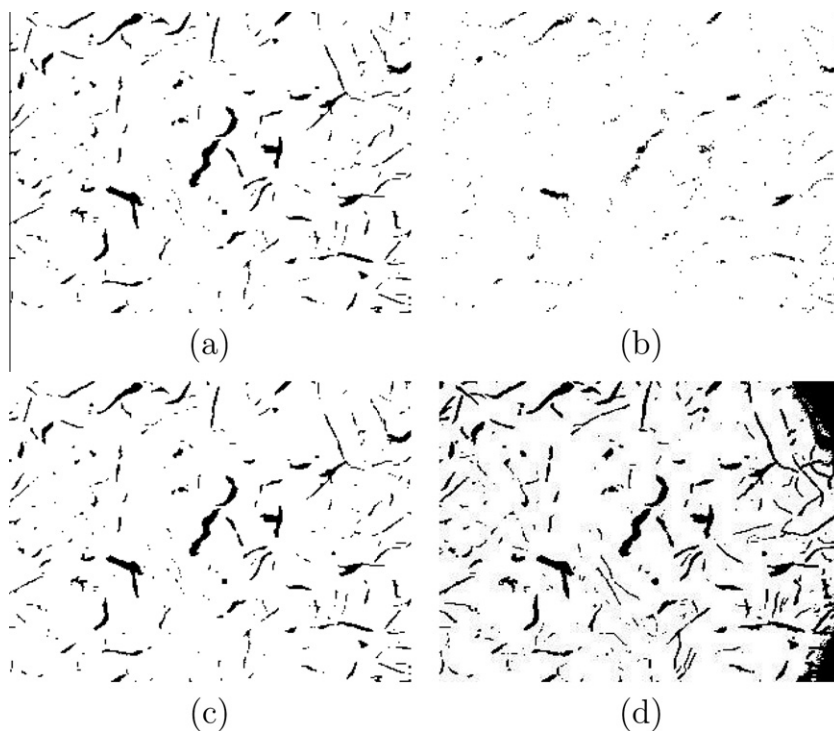
Fig. 4. Characterization results regarding the original image in Fig. 3a: (a) OPF, (b) SVM-RBF, (c) Bayes and (d) Otsu's computer techniques.

Table 5
Mean UIQI and execution times in seconds after cross-validation for OPF, SVM-RBF and Bayes based classifiers and for Otsu's method with respect to the second round of experiments. (The bolded values stand for the most accurate classifiers.)

Classifier	Cast iron	UIQI	Training [s]	Testing [s]
OPF	Gray	**0.9605 ± 0.0031**	**5.07**	**20.02**
Bayes	Gray	**0.9631 ± 0.0024**	**0.43**	**68.57**
SVM-RBF	Gray	0.7124 ± 0.0033	3.96	18.04
Otsu	Gray	−0.0837		0.01

Table 6
Values of χ^2 computed for all pairs of computer methods for the extra round of experiments with respect to the gray cast iron (Fig. 3a). The bolded values stand for similar classifiers.

χ^2	Bayes	OPF	SVM-RBF	Otsu
Bayes	–	**3.71**	2346.0	6493.5
OPF	**3.71**	–	2339.0	6454.6
SVM-RBF	2346.0	2339.0	–	1967.7
Otsu	6493.5	6454.6	1967.7	–

quantification has been paramount. Therefore, this paper has as main contribution a comparison among three state-of-the-art supervised computer classifiers: Support Vector Machine, Optimum-Pat Forest and Bayesian based classifiers, and also against the well-known Otsu's method. In addition, to the best of our knowledge, we are the first to applied OPF, SVM and Bayesian based computer classifiers into this field.

We conducted the experiments as follows: we compared the OPF, SVM and Bayesian based classifiers and Otsu's method for the gray, malleable and nodular cast irons automatic characterization. Each sample of the dataset, i.e., each image pixel, was described by 18 Gabor texture features and its original gray value in order to be characterized by the computer classifiers under comparison. In this experimental round, we used 50% of the gray cast iron image for training and the remaining 50% for characterization, i.e., classification, purpose. In regard to the nodular and malleable cast irons, we employed 10% for training and 90% for characterization. In regard to the gray and malleable cast irons, the UIQI accuracy and the statistical analysis confirmed that the best results were obtained by the Otsu's method, and that for the nodular cast iron the most accurate methods were the Bayesian and OPF based classifiers, which obtained similar results according to the χ^2 statistical analysis. From the experimental findings, we can conclude that computer classifiers studied are suitable for the automatic characterization of graphite particles of cast irons in metallographic images, since they overcome successfully the traditional problems inherent to the visual inspection methods. Although the Otsu's method has outperformed the Bayesian, SVM-RBF and OPF based classifiers in 2 of the 3 datasets used, this good performance has been questioned in more complex situations. In fact, the Otsu's method is efficient when applied on simply images, but not so effective when used in more complex images, which can be easily found in several industrial applications. Additionally, this method does not present the ability to learn from the previous experience, as the machine learning techniques can present. As such, this means that the Otsu's method perform a *blind* characterization of each input image in an independent manner, without addressing any prior knowledge about the structures involved. Therefore, the use of machine learning techniques for image classification in industrial applications has been demonstrated to be an outstanding procedure, as well as to employ the OPF classifier in this context.

Acknowledgments

References

Albuquerque, V. H. C., Cortez, P. C., de Alexandria, A. R., & Tavares, J. M. R. S. (2008). A new solution for automatic microstructures analysis from images based on a backpropagation artificial neural network. *Nondestructive Testing and Evaluation, 23*(4), 273–283.

Albuquerque, V. H. C., de Alexandria, A. R., Cortez, P. C., & Tavares, J. M. R. S. (2009). Evaluation of multilayer perceptron and self-organizing map neural network topologies applied on microstructure segmentation from metallographic images. *NDT&E International, 42*(7), 644–651.

Albuquerque, V. H. C., Papa, J. P., Falcão, A. X., Filho, P. P. R., & Tavares, J. M. R. S. (2010). Application of optimum-path forest classifier for synthetic material porosity segmentation. In *Proceedings of the 17th international conference on systems, signals and image processing* (pp. 57–60).

Albuquerque, V. H. C., Filho, P. P. R., Cavalcante, T. S., & Tavares, J. M. R. S. (2010). New computational solution to quantify synthetic material porosity from optical microscopic images. *Journal of Microscopy, 240*(1), 50–59.

Albuquerque, V. H. C., Tavares, J. M. R. S., & Cortez, P. C. (2010). Quantification of the microstructures of hypoeutectic white cast iron using mathematical morphology and an artificial neural network. *International Journal of Microstructure and Materials Properties, 5*(1), 52–64.

Allène, C., Audibert, J. Y., Couprie, M., Cousty, J., & Keriven, R. (2007). Some links between min-cuts, optimal spanning forests and watersheds. In *Proceedings of the international symposium on mathematical morphology, MCT/INPE* (pp. 253–264).

Boser, B. E., Guyon, I. M., & Vapnik, V. N. (1992). A training algorithm for optimal margin classifiers. In *Proceedings of the 5th workshop on computational learning theory* (pp. 144–152). New York, NY, USA: ACM Press.

Callister, W. D. (2006). *Materials science and engineering: An introduction.* John Wiley & Sons Inc..

Collobert, R., & Bengio, S. (2001). SVMTorch: Support vector machines for large-scale regression problems. *Journal of Machine Learning Research, 1,* 143–160.

Cortes, C., & Vapnik, V. (1995). Support vector networks. *Machine Learning, 20,* 273–297.

Dijkstra, E. W. (1959). A note on two problems in connexion with graphs. *Numerische Mathematik, 1,* 269–271.

Duda, R. O., Hart, P. E., & Stork, D. G. (2000). *Pattern classification* (2nd ed.). Wiley Interscience.

Falcão, A. X., Stolfi, J., & Lotufo, R. A. (2004). The image foresting transform theory, algorithms, and applications. *IEEE Transactions on Pattern Analysis and Machine Intelligence, 26*(1), 19–29.

Feichtinger, H. G., & Strohmer, T. (1997). *Gabor analysis and algorithms: Theory and applications* (1st ed.). Boston: Birkhauser.

Filho, P. P. R., Cavalcante, T. S., Albuquerque, V. H. C., & Tavares, J. M. R. S. (2010). Brinell and vickers hardness measurement using image processing and analysis techniques. *Journal of Testing and Evaluation, 38*(1), 1–7.

Gomes, O. F. M., & Paciornik, S. (2005). Automatic classification of graphite in cast iron. *Microscopy and Microanalysis, 11*(4), 363–371.

Jaynes, E. T. (2003). *Probability theory: The logic of science.* Cambridge University Press.

Kuncheva, L. I. (2004). *Combining pattern classifiers: methods and algorithms.* Wiley-Interscience.

Li, T. S. (2009). Applying wavelets transform and support vector machine for copper clad laminate defects classification. *Computers & Industrial Engineering, 56*(3), 1154–1168.

Liao, T. W. (2008). Classification of weld flaws with imbalanced class data. *Expert Systems with Applications, 35*(3), 1041–1052.

Metwalli, S. M. (1986). Industrial applications of computer image processing. *Computers & Industrial Engineering, 11,* 608–612.

Otsu, N. (1979). A threshold selection method from gray-level histograms. *IEEE Transactions on Systems, Man and Cybernetics, 9*(1), 62–66.

Papa, J. P., Suzuki, C. T. N., & Falcão, A. X. (2009). LibOPF: A library for the design of optimum-path forest classifiers, software version 2.0, 2009. Available at: <http://www.ic.unicamp.br/afalcao/LibOPF>.

Papa, J. P., Falcão, A. X., & Suzuki, C. T. N. (2009). Supervised pattern classification based on optimum-path forest. *International Journal of Imaging Systems and Technology, 19*(2), 120–131.

Papa, J. P., Gutierrez, M. E. M., Nakamura, R. Y. M., Papa, L. P., Vicentini, I. B. F., & Vicentini, C. A. (2011). Automatic classification of fish germ cells through optimum-path forest. In *2011 Annual international conference of the IEEE engineering in medicine and biology society* (pp. 5084–5087). IEEE Press.

Pisani, R. J., Riedel, P., Ferreira, M., Marques, M., Namakura, R. Y. M., & Papa, J. P. (2011). Land use image classification through optimum-path forest clustering. In *Proceedings of the IEEE international geoscience and remote sensing symposium* (pp. 826–829). IEEE Press.

Pisani, R. J., Riedel, P., Gomes, A., Nakamura, R. Y. M., & Papa, J. P. (2011). Is it possible to make pixel-based radar image classification user-friendly? In *Proceedings of the IEEE international geoscience and remote sensing symposium* (pp. 4304–4307). IEEE Press.

Scholköpf, B., & Smola, A. J. (2002). *Learning with kernels.* Cambridge, MA: MIT Press.

Scozzafava, A., Tomesani, L., & Zucchelli, A. (2004). Image analysis automation of spheroidal cast iron. *Journal of Materials Processing Technology, 153–154,* 853–859.

Sezgin, M., & Sankur, B. (2004). Survey over image thresholding techniques and quantitative performance evaluation. *Journal of Electronic Imaging, 13*(1), 116–146.

Torres-Treviño, L. M., Reyes-Valdes, F. A., López, V., & Praga-Alejo, R. (2011). Multi-objective optimization of a welding process by the estimation of the pareto optimal set. *Expert Systems with Applications, 38*(7), 8045–8053.

Valavanis, I., & Kosmopoulos, D. (2010). Multiclass defect detection and classification in weld radiographic images using geometric and texture features. *Expert Systems with Applications, 37*(12), 7606–7614.

Vapnik, V. N. (1999). An overview of statistical learning theory. *IEEE Transactions on Neural Networks, 10,* 988–999.

Wang, Z., & Bovik, A. C. (2002). A universal image quality index. *IEEE Signal Processing Letters, 9*(3), 81–84.

West, T. D. (2008). *Metallurgy of cast iron.* Cleveland Printing & Pub. Co..

Yoon, Y. G., Lee, S. L., Chung, C. W., & Kim, S. H. (2008). An effective defect inspection system for polarized film images using image segmentation and template matching techniques. *Computers & Industrial Engineering, 55*(3), 567–583.

Zapata, J., Vilar, R., & Ruiz, R. (2011). Performance evaluation of an automatic inspection system of weld defects in radiographic images based on neuro-classifiers. *Expert Systems with Applications, 38*(7), 8812–8824.